The 8th European Congress on Computational Methods in Applied Sciences and Engineering
ECCOMAS Congress 2022
5-–9 June 2022, Oslo, Norway

A DEM-COUPLED OPENFOAM SOLVER FOR MULTIPHYSICS SIMULATION OF ADDITIVE MANUFACTURING PROCESS: DEVELOPMENT AND VALIDATION

NAVID AMINNIA[1], ALVARO ANTONIO ESTUPINAN DONOSO[2] AND BERNHARD PETERS[3]

Faculté des Sciences, de la Technologie et Médecine (FSTM)
Université du Luxembourg
Campus Belval, 6, avenue de la Fonte, L-4364 Luxembourg
[1] e-mail: navid.aminnia@uni.lu, [2] alvaro.estupinan@uni.lu, [3] bernhard.peters@uni.lu

Key words: CFD-DEM Coupling, Additive Manufacturing, Multiphase Flow, Marangoni Convection

Abstract. Powder-based additive manufacturing technologies, specifically selective laser melting, are challenging to model due to the complex, interrelated physical phenomena that are present on multiple spatial scales, during the process. A key element of such models will be the detailed simulation of flow and heat transfer throughout the melt pool that is formed when the powder particles melt. Due to the high-temperature gradients that are generated inside the melt pool, the Marangoni force plays a key role in governing the flows inside the melt pool and deciding its shape and dimensions. On the other hand, the mass and heat transfer between the melt and the powder also has a significant role in shaping the melt pool at the edges. In this study, we modified an OpenFOAM solver (icoReactingMultiphaseInterFoam) coupled with an in-house developed DEM code known as eXtended Discrete Element Method or XDEM which models the dynamics and thermodynamics of the particles. By adding the Marangoni force to the momentum equation and also defining a laser model as a boundary condition for liquid-gas interface, the solver is capable of modeling the selective laser melting process from the moment of particle melting to the completion of the solidified track. The coupled solver was validated with an ice packed bed melting case and was used to simulate a multi-track selective laser melting process.

1 Introduction

In recent years, powder-bed fusion technology has become more popular, leading to a variety of modeling approaches [1]. At the macroscopic scale, multiphysics models have been developed to study melting and solidification phenomena caused by a moving heat source above a powder bed [2]. Several studies have shown that the fluid flow within the melt pool, particularly Marangoni convection and recoil pressure, can lead to the development of critical defects such as porosity, spattering, denudation, and balling [2]. These studies mainly differ in the numerical methods they have used and the details of the physics that they have incorporated into their models [3]. Some authors have implemented models such as Marangoni convection, recoil

pressure [4] or evaporative [2] and convective cooling [5] of the melt pool while others may have excluded some of them.

An important part of the AM process involves the absorption of heat from the laser or electron beam and the distribution of this heat in the powder bed. Treatment of laser radiation and heat conduction in the powder is connected to the treatment of the powder bed[3]. Some studies consider the powder bed as a continuum and some consider individual particles. The continuum models have commonly considered laser as a spatially-varying heat flux with a Gaussian distribution. In these studies, laser heat profile is either constant in depth-direction or varies based on a correlation [6]. In continuum models, thermal conductivity is considered an effective value for the whole powder bed. For instance, Gustarov et. al [7] considered the effective thermal as a fixed small value below melting temperature and a greater value for the melt. However recently, there has been a shift towards using discrete powder bed models. Ganeriwala and Zohdi [8] used a Discrete Element Method (DEM) to model the powder bed and a finite difference method for the substrate. They considered a gaussian distribution for the laser with exponentially decaying radiation in the depth. In these models, the gas is not considered a second phase, therefore, only the contact point heat conduction is accounted for[3].

In the present work, a CFD-DEM coupled model is developed and validated for the simulation of the selective laser melting process. The CFD model is based on the VOF method and considers the gas phase between the particles and calculates its heat transfer with the powder bed. The DEM model simulates a discrete powder bed with particles subjected to convective, conductive, and radiative heat transfer.

2 METHODOLOGY

2.1 Discrete element method

The particles are treated as a discrete solid phase in an in-house DEM code known as the eXtended Discrete Element Method (XDEM [9]). XDEM predicts both dynamics and thermodynamic states of the particular system. The dynamic module calculates the particle position, velocity, and acceleration whereas the temperature, melting rate, and shrinkage of the particle is calculated within the conversion module.

2.1.1 Dynamic module

The discrete element method used in the dynamic module is based on the soft-sphere contact model where the particles are assumed deformable and may overlap. The magnitude of this overlap depends on the contact force calculated by the force-displacement law. The particle hardness is described by Young's modulus, and the particle kinetic energy dissipation is characterized by a dampener and/or a dashpot. Detailed descriptions of these calculations and the equations below, can be found in a previous work [10]. The translational and rotational movements of the particles are described by Newton's second law of motion and Euler's rotation equation:

$$m_i \frac{d\vec{v_i}}{dt} = m_i \frac{d^2\vec{X}_i}{dt^2} = \vec{F_i^c} + \vec{F_i^g} + \vec{F_i^{ext}} \tag{1}$$

$$I_i \frac{d\vec{\omega_i}}{dt} = \sum_{j=1}^{n} \vec{M_{i,j}} \tag{2}$$

The contact force $\vec{F_i^c}$ is the summation of all normal $\vec{F_{i,j}^{c,n}}$ and tangential $\vec{F_{i,j}^{c,t}}$ forces that are exerted by other particles when they collide. $\vec{F_i^g}$ is the graviational force. $\vec{F_i^{ext}}$ is the summation of all external forces acting on the particle, including the drag force F_d and the buoyancy force F_B from the ambient fluid.

2.1.2 Conversion module

Conversion module solves the momentum, mass, energy (and species) conservation equation within the particles which are radially discretized. Mass conservation equation is solved for the fluid that is present within the particle pores:

$$\frac{\partial}{\partial t}\left(\epsilon_f \rho_f\right) + \vec{\nabla} \cdot \left(\epsilon_f \rho_f \vec{v_f}\right) = \dot{m}_{s,f} \tag{3}$$

A One-dimensional transient energy equation is solved for all the particles:

$$\frac{\partial \rho c_p T}{\partial t} = \frac{1}{r_n}\frac{\partial}{\partial r}\left(r^n \lambda_{eff}\frac{\partial T}{\partial r}\right) - r^n\left(\vec{v}\rho_f c_{p_f} T\right) + \sum_{k=1}^{l} \dot{\omega}_k H_k \tag{4}$$

These governing equation are subjected to the ollowing boundary conditions:

$$-\lambda_{eff}\frac{\partial T}{\partial r}\bigg|_{r=0} = 0 \tag{5}$$

$$-\lambda_{eff}\frac{\partial T}{\partial r}\bigg|_{r=R} = \alpha(T_R - T_\infty) + q''_{rad} + q''_{cond} + q''_{laser} \tag{6}$$

$$-D_{i,eff}\frac{\partial \rho_i}{\partial r}\bigg|_{r=R} = \beta_i\left(\rho_{i,R} - \rho_{i,\infty}\right) \tag{7}$$

q''_{laser} is surface heat flux coming from the laser. The formulation is consistent with the laser formulation of the CFD model presented in equation **??**, other than it also considers a heat profile in depth direction according to [8]. The aformentioned equations and the conversion model are described in detail in [11, 10].

The melting process involves interfacial mass transfer from the solid phase to the liquid phase. The rate of this transfer is denoted as melting rate $\dot{m}$ in equation 3 and can be calculated based on the energy balance relation. The melting rate is defined by the ratio of the available enthalpy above melting temperature to the latent enthalpy required for melting L_f:

$$\dot{m}_{s,f} = \begin{cases} \frac{(h-h_m)}{L_f \Delta t} & h \geq h_m \\ 0 & h < h_m \end{cases} \tag{8}$$

The melting rate ($\dot{m}_{s,f}$) is transferred to the CFD field by introducing a source term in the fluid continuity equation Eq 10.

2.2 Computational fluid dynamics

The motion of fluid is calculated using Volume of Fluid (VOF) method where the continuity, momentum and energy equations are solved for two or more immiscible phases. Consequently, the resulting velocity ($\vec{v_f}$) , density (ρ) and temperature (T) are weight-averaged among all fluid phases:

Volume of fluid equation:

$$\frac{\partial \gamma}{\partial t} + \vec{\nabla}.(\gamma U) = 0 \tag{9}$$

Conservation of mass:

$$\frac{\partial}{\partial t}\left(\epsilon_f \rho_f\right) + \vec{\nabla} \cdot \left(\epsilon_f \rho_f \vec{v_f}\right) = \dot{m}_{s,f} \tag{10}$$

Where ϵ is the local porosity (the volume fraction available for the fluid phase) and $\dot{m}_{s,f}$ is the mass source due to the phase change of solid particles to fluid.

Conservation of momentum:

$$\frac{\partial}{\partial t}\left(\epsilon \rho_f \vec{v}_f\right) + \nabla \cdot \left(\epsilon \rho_f \vec{v}_f \vec{v}_f\right) = -\epsilon \nabla p + \epsilon \mu \nabla^2 \vec{v}_f + S_U + S_p + F_s \tag{11}$$

$$S_U = \rho \vec{g} \beta (T - Tref) - \frac{C(1-\gamma_l)}{{\gamma_l}^3 + e_0} \vec{v_f} \tag{12}$$

p, μ denote respectively the pressure field and viscosity. S_U expresses the momentum sources defined in the model. The first term (thermal buoyancy) uses the concept of Boussinesq approximation where $\vec{g}$ is the gravitational acceleration constant and β the thermal expansion coefficient. The second term (momentum sink) expresses the momentum in the mushy zone and is the function of liquid volume fraction γ_l, which represents liquid for $\gamma_l = 1$ and solid for $\gamma_l = 0$. C is a constant that is chosen to be large enough (10^6) to create a large momentum sink in solid. While e_0 is a small constant (10^{-3}) to avoid division by zero. This term acts as a large momentum sink in the solid region while in the liquid region it vanishes.

$$S_p = \epsilon \rho_f \vec{A_c} - \epsilon \rho_f \Omega_c \vec{v}_{f_c} \tag{13}$$

S_p denotes the source terms introduced from the particle. $\vec{A_c}$ (m/s^2) and Ω ($1/s$) are the linear and angular acceleration exerted by the particles on the considered control volume.

$\vec{F_s}$ is the volumetric smeared surface force based on Continum surface force (CSF) method [12], that is applied on gas-liquid interface:

$$\vec{F_s} = \left[\sigma \kappa \vec{n} + \frac{d\sigma}{dT}(\nabla T - \vec{n}(\vec{n}.\vec{\nabla} T))\right] |\nabla \gamma| \frac{2\rho}{\rho_1 + \rho_2} \tag{14}$$

The equation is composed of a normal and a tangentional component. The tangentioal component is created due to a high surface tension gradient on the gas-liquid interface. In the applications such as laser welding and additive manufacture where the surface of the melt may experience a high temperature gradient, this component can become the dominant term in the momentum equation. The term $(\nabla T - \vec{n}(\vec{n}.\vec{\nabla} T))$ gives the tangentional component of the temperature gradient. σ is surface tension coefficient, κ is the curvature, $\vec{n}$ the surface normal

vector. $|\nabla\gamma|$ is the gradient of volume fraction and serves as the Brackbill delta function and the term $\frac{2\rho}{\rho_1+\rho_2}$ plays a role in redistributing the forces toward the heavier phase (the liquid) so that high accelerations in air-filled cells are avoided [12] .

Conservation of energy:

$$\frac{\partial}{\partial t}\left(\epsilon\rho_f c_{p_f} T\right) + \nabla\cdot\left(\epsilon\rho_f c_{p_f}\vec{v}_f T\right) = \nabla\cdot\left(\epsilon\lambda_f\nabla T_f\right) + S_p + S_{laser} \tag{15}$$

c_{p_f} and λ_f are the average specific heat and thermal conductivity of the fluid mixture. These physical properties along with the density are calculated as volume-weighted averages of the phases present in the control volume under consideration. S_p is the heat source introduced by the particle (XDEM) and includes the thermal convection and mass flux energy of the melt (the enthalpy that is being introduced along with $\dot{m}_{s,f}$ in Eq 8. S_{laser} is the heat source from the laser. A formulation of the CSF method [12] was used here to define the surface heat flux of the laser as a volumetric heat source on the gas-liquid interface.

$$S_{laser} = Q_{laser}\frac{\rho c_p}{\rho_1 c_{p_1} + \rho_2 c_{p_2}} \tag{16}$$

$$Q_{laser(W/m^3)} = q''_{laser(W/m^2)}\,|\nabla\gamma| \tag{17}$$

$$q_{laser} = \frac{2\eta P_{laser}}{\pi R^2} exp\left(-2\frac{(x-x_0-\nu t)^2 + (y-y_0)^2}{R^2}\right) \tag{18}$$

Eq 16 redistributes the heat source over the phase with higher ρc_p, which is liquid at the gas-liquid interface. Eq 17 shows the adaptation of the CSF method to define the laser as a volumetric surface heat source based on the idea proposed by [13]. In Eq , η is absorption cofficient which is considered as constant. P_{laser} is the laser power and R is the laser beam radius. x_0 and y_0 are the starting coordinates of the laser beam and ν is the laser beam velocity.

2.3 Numerical Implementation

The CFD-DEM coupling is achieved through a conventional staggered approach. The CFD model was developed using the OpenFOAM library and is based on `icoReactingMultiphaseInterFoam` solver. The new solver which adopts new features is now called `marangoniIcoReactingMultiphaseInterFoam`. The XDEM and OpenFOAM libraries are linked together and run via a single executable. The simulation starts after running the executable. First, the XDEM is initialized and the boundary conditions of the particles are defined. A volume fraction field for the particle phase is calculated by XDEM based on the location of the particle and the mesh structure of the CFD case. The particle phase would not enter the CFD conservation equations though. This information is only used for solid-to-liquid mass transfer.

At the beginning of each iteration, XDEM calculations are performed. Based on the calculations in XDEM, heat, mass and momentum sources are written as OpenFOAM fields. The OpenFOAM simulation starts its iterations considering the source terms. Heat and momentum sources are read via the `fvOptions` dictionary. However, mass source is defined as a `massTransferModel` for solid (particle phase) to liquid. The fluid governing equations are solved in the

OpenFOAM solver and the new velocity, pressure, temperature, density, specific heat, and viscosity fields are calculated. Then the simulation moves to the next time step and these updated fields are read by XDEM and used to calculate the new boundary conditions of the particles.

3 RESULTS AND VALIDATION

This research was comprised of two main parts. In the first part, a CFD model was developed that was capable of considering all the dominant transport phenomena that are at play in a selective laser melting process. The second part was to develop a coupling of the CFD solver with XDEM which is responsible for modeling the dynamics and the thermodynamics of the powder particles in the aforementioned additive manufacturing process.

3.1 CFD model Validation

The CFD model was developed into an OpenFOAM solver named `marangoniIcoReacting-MultiphaseInterfoam`. As described in section 2.2 this model solves for N incompressible, non-isothermal immiscible fluids with phase change using a VOF method. This model can consider the Marangoni convection and laser heat source on the surface of liquids and solids. Therefore, in the first step, the model is validated by simulating a laser spot welding experiment [14].

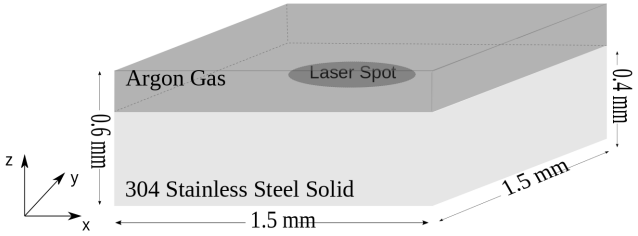

Figure 1: Illustration of the simulation domain. A stainless steel block and argon as shielding gas

3.1.1 Laser spot welding simulation

The laser welding process has many mutual physical phenomena with selective laser melting. A melt pool is created due to laser radiation on a solid surface and interacts with the laser. The Marangoni convection is a dominant force in generating a circulatory flow inside the melt pool which decides its shape and dimensions.

The physical properties that are used in the model are adapted from the values reported by the experiment article and are listed in table 2 [14]. A schematic of the laser welding specimen which is also the geometry for the simulation is presented in figure **??**. In the simulation, a $1.5mm \times 1.5mm \times 0.4mm$ stainless steel block with a bulk of argon gas on top, is subjected to laser radiation for 3ms. Due to high temperatures (up to 3000K) at the laser incident point, the surface of the melt experiences strong surface tension gradients. This results in the generation of a strong circulatory flow inside the melt pool. Figure 2 shows the evolution of the melt pool over time. The isoline of $1697K$ indicates the melt pool border. Inside the melt pool, the velocity

vectors are shown. As time passes and more heat from laser radiation is accumulated on the melt surface, the temperature difference from the laser incident point to the edges of the melt pool increases. It can be observed that the ratio of this temperature difference at two consecutive time steps is greater than the ratio of the melt pool widths. This means an increase in temperature gradient on the melt surface which in turn means a stronger Marangoni convection. Therefore as time passes by, stronger Marangoni flow is observed which is characterized by larger velocity vectors and circulatory flows. The right-hand side ciculatory flow is clearly distinguishable in the melt pool of the time t = 3 ms. The flow on the surface is directed from the region with low surface tension (high temperature) to the region with high surface tension. Therefore on the right-hand side of the melt pool the circulatory flow is clockwise while on the left-hand it is anti-clockwise.

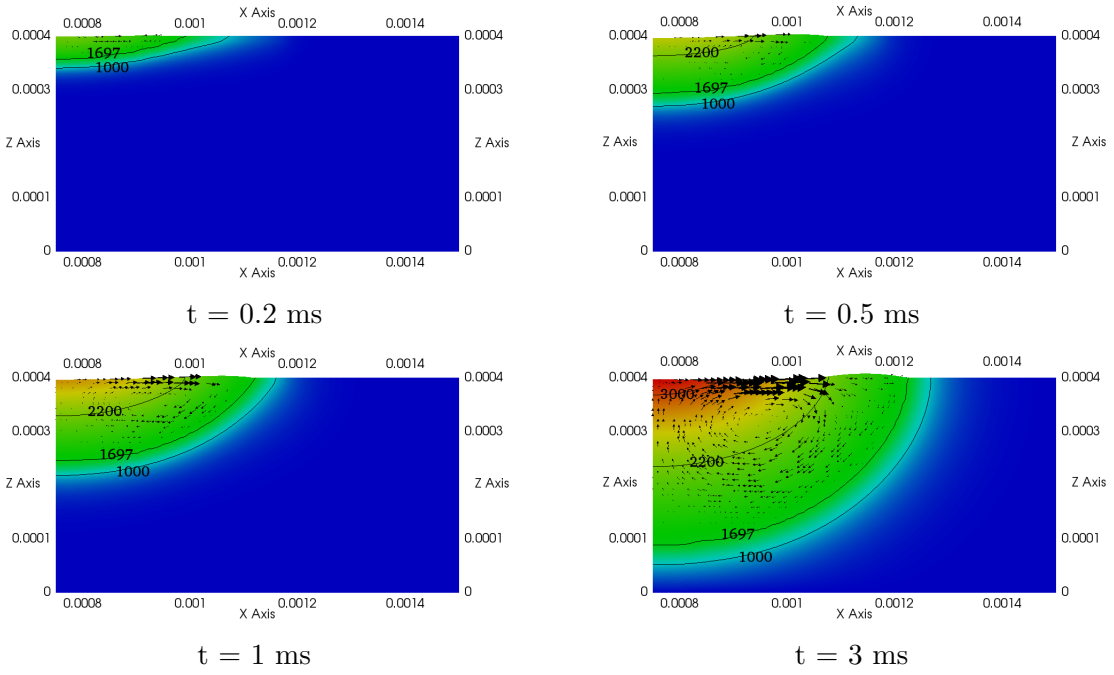

Figure 2: Evolution of melt pool over time. Figures show the right half of an XZ cross section of the steel block at Y = 0.5 mm which coincides with the laser incident point

The simulation results are compared with previous studies and the experiment results are in table 3.1.1. The dimensions of the melt pool are commonly used as the criteria for validating the result because they are directly affected by the magnitude of the temperature gradients and Marangoni force.

Research	Scope	Half Width (mm)	Depth (mm)
He et. al [14]	Experiment	0.47	0.26
Tan et. al [15]	Simulation	0.44	0.25
Our work	Simulation	0.44	0.25

Table 1: Comparison of the melt pool dimensions with experiment and another simulation

3.2 CFD-DEM Coupling Validation

3.2.1 One sphere of ice in a tank of water

Shukla et. al [16] set up a cold model experiment using ice and water to study the melting of steel straps in the high-temperature liquid iron melt. This study gives an insight into the convection melting of solid inside a pool of liquid. We have recreated this physical setup in our model to validate the convection and melting of the CFD-DEM coupling that is designed for the simulation of additive manufacturing processes.

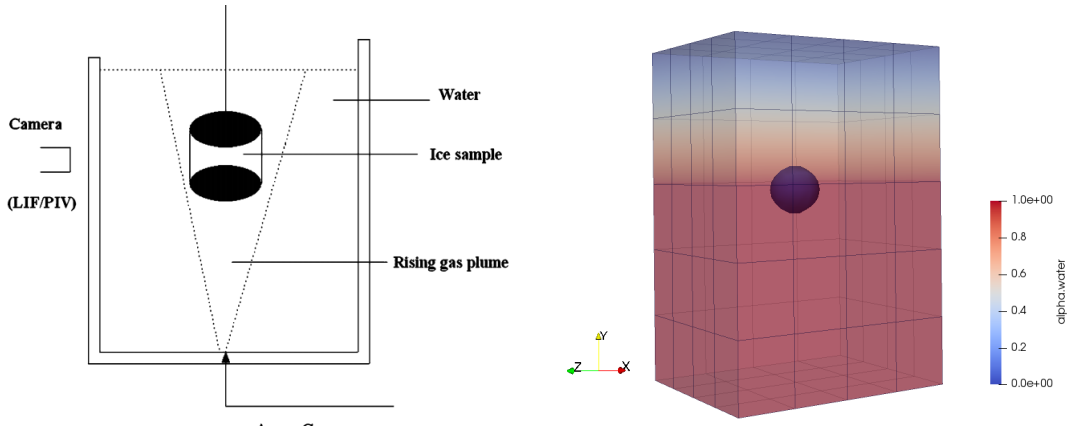

Expeimental setup [16] Simualtion setup

Figure 3: A schematic of the experimental setup used by Shukla et. al (left) and the simulation setup in OpenFoam (right) nearly two-thirds of the tank is filled with water and the rest with gas

In the original experiment, to study natural convection, a bulk of ice in the shape of a sphere was left floating in a tank of water at $20°C$ and the variations of the radius over time were recorded. In other experiments, they also added a gas inflow to observe the effects of forced convection. However we did not perform simulation on those experiments because they are out of the scope of our interest. Figure 3 (a) shows the experimental setup and figure (b) shows the simulation domain that was created based on that setup.

Figure 4 compares the experiment's reported ice radius over time to the simulation results. The ice radius over time characterizes the melting rate of the particle which is dominantly affected by the heat transfer of the particle. The objective of this simulation was to validate the melting model and convective heat transfer between XDEM and the CFD model.

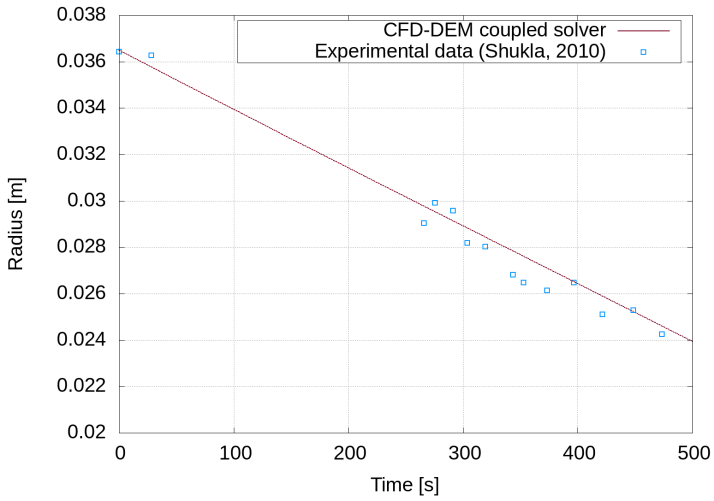

Figure 4: Comparison of the ice radius variations in the experiment and the simulation

3.2.2 Packed bed of ice in flowing water

The second validation case is based on an experiment performed by Hao and Tao [17] to study the convective melting of a granular packed bed of ice in flowing water. The objective here is to validate the heat, mass, and momentum source transfer between XDEM and the CFD model. To obtain this goal, the model is anticipated to predict the movements of the packed bed, and shrinkage in the size of the bulk of particles.

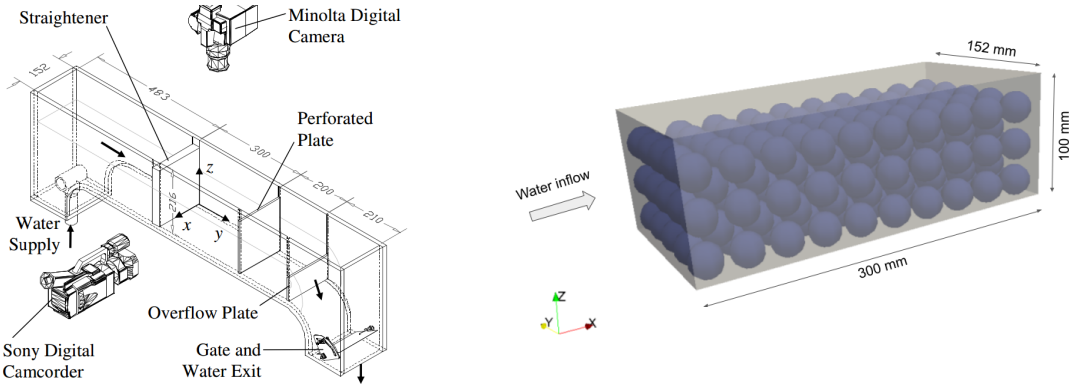

(a) Experimental setup [17] (b) Simulation setup

Figure 5: A schematic of the experimental setup used by Hao (left) and our simulation setup (right)

In the experiment carried out by Hao, the packed bed was placed in a water channel but restrained by two perforated plates. In our simulation, the plates are modeled as walls on the two sides of the packed bed. They repeat the experiment for three different inlet velocities and for each case, the total mass of the packed bed is calculated based on the water level rise in

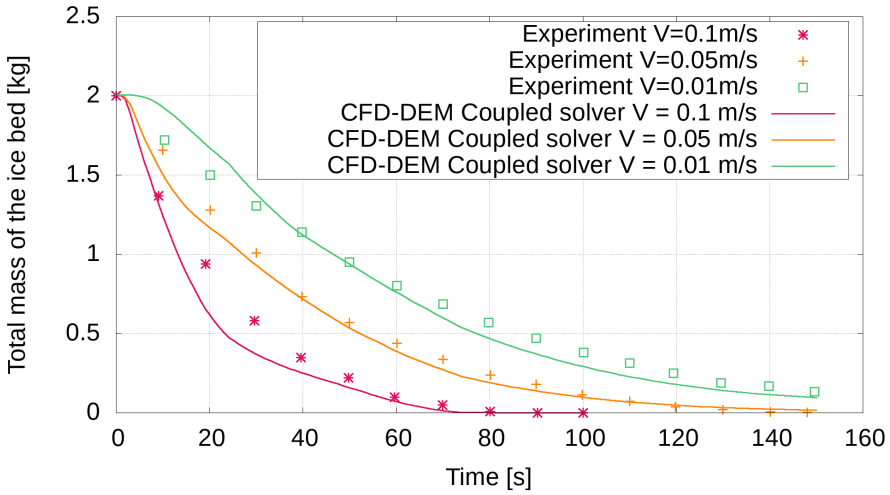

Figure 6: Comparison of total mass of the ice packed bed through time for three different inlet velocities

the channel. As can be seen in figure 5 a camera is installed, pointing at the ice packed bed to record the movements of the ice particles. We have used the mass variation report and camera images as the basis for our validation.

The results of the validation are shown in figure 6. It can be observed that for the three different velocities the degree of agreement between the simulation and experiment are different. This is because the parameters used for the heat transfer laws are sensitive to the fluid velocity. Therefore for each simulation setup, heat transfer parameters should be set based on the physical process at hand. Whereas in this simulation for the sake of comparison all the cases use Yang heat transfer law [18] to estimate the convective heat transfer between the particles and the surrounding water.

Figure 7 shows the evolution of the ice packed bed with time. Figures 7 (a) and (c) show the photos taken by the camera in the experimental setup and figures (b) and (d) show the result of the simulation. The water flow pushes the ice particles towards the right perforated plane. With time, the particles, are subjected to warm water, melt and shrink. We can see the exact same behaviour from the simulated packed bed (Figure 7).

4 DISCUSSIONS

The objective of this research is to develop a CFD-DEM coupled model that includes the required features for a selective laser melting model. The focus of this article is the development and the validation of the model. Therefore the different milestones were defined for incremental development of the model. The first milestone was developing a suitable CFD model and it was carried out in the form of a new OpenFOAM solver. The next one was to couple the developed CFD solver to XDEM. The main challenge in this part of the research was to ensure that transfer and implementation of the source terms between XDEM and OpenFOAM were done properly. Therefore this article is mainly devoted to the development, method description, and the results of the validations. In future works, the CFD-DEM coupling will be applied to a selective laser melting process to predict the melt pool transport phenomena and investigate

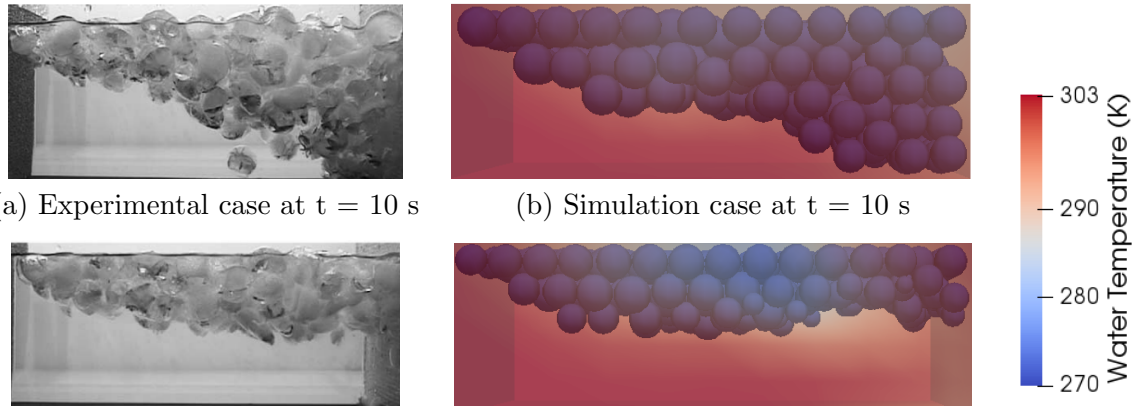

(a) Experimental case at t = 10 s (b) Simulation case at t = 10 s

(c) Experimental case at t = 30 s (d) Simulation case at t = 30 s

Figure 7: Floating packed packed subjected to a warm inflowing water. (a) experimental result [17] (b) simulation result. $T_{in} = 303$ K, $V_{in} = 0.07$ m/s

the effect of different parameters.

5 CONCLUSIONS

In this study the preliminary steps to develop a Lagrangian-Eulerian model for an additive manufacturing process, more specifically, the selective melting process was described and discussed.

The CFD model was developed in OpenFOAM, in the form of a new solver, *marangoniIcoReactingMultiphaseInterFoam* which is a VOF incompressible solver of N phases with phase-change and considers the Marangoni convection and has a laser model implemented. The solution was validated and compared to a laser spot welding experiment and the results showed agreement with the values reported by the experiment.

Based on the newly developed solver a DEM-coupled solver was developed that couples the solver to XDEM. XDEM reads the physical properties and field data (temperature, velocity, etc.) from OpenFOAM, solves the dynamics and thermodynamics of the particles, and transfers the resulting heat, mass, and momentum sources to the OpenFOAM solver. The coupled solver was validated against two experiments. The first experiment involved a single ice particle subjected to natural convection in a tank of water, and the second involved a packed bed of ice flowing through a channel. The results ensured us that the model is ready and reliable to be applied to an additive manufacturing process.

References

[1] T DebRoy et al. “Metallurgy, mechanistic models and machine learning in metal printing”. In: *Nature Reviews Materials* 6.1 (2021), pp. 48–68.

[2] Saad A Khairallah et al. “Laser powder-bed fusion additive manufacturing: Physics of complex melt flow and formation mechanisms of pores, spatter, and denudation zones”. In: *Acta Materialia* 108 (2016), pp. 36–45.

[3] Peter S Cook and Anthony B Murphy. "Simulation of melt pool behaviour during additive manufacturing: Underlying physics and progress". In: *Additive Manufacturing* 31 (2020), p. 100909.

[4] Alexander Klassen, Thorsten Scharowsky, and Carolin Körner. "Evaporation model for beam based additive manufacturing using free surface lattice Boltzmann methods". In: *Journal of Physics D: Applied Physics* 47.27 (2014), p. 275303.

[5] Zhidong Zhang et al. "3-Dimensional heat transfer modeling for laser powder-bed fusion additive manufacturing with volumetric heat sources based on varied thermal conductivity and absorptivity". In: *Optics & Laser Technology* 109 (2019), pp. 297–312.

[6] Jung-Ho Cho and Suck-Joo Na. "Implementation of real-time multiple reflection and Fresnel absorption of laser beam in keyhole". In: *Journal of Physics D: Applied Physics* 39.24 (2006), p. 5372.

[7] AV Gusarov et al. "Model of radiation and heat transfer in laser-powder interaction zone at selective laser melting". In: *Journal of heat transfer* 131.7 (2009).

[8] Rishi Ganeriwala and Tarek I Zohdi. "A coupled discrete element-finite difference model of selective laser sintering". In: *Granular Matter* 18.2 (2016), pp. 1–15.

[9] Bernhard Peters et al. "XDEM multi-physics and multi-scale simulation technology: Review of DEM–CFD coupling, methodology and engineering applications". In: *Particuology* 44 (2019), pp. 176–193.

[10] Mehdi Baniasadi, Maryam Baniasadi, and Bernhard Peters. "Coupled CFD-DEM with heat and mass transfer to investigate the melting of a granular packed bed". In: *Chemical Engineering Science* 178 (2018), pp. 136–145.

[11] Bernhard Peters. "Thermal conversion of solid fuels". In: (2002).

[12] Jeremiah U Brackbill, Douglas B Kothe, and Charles Zemach. "A continuum method for modeling surface tension". In: *Journal of computational physics* 100.2 (1992), pp. 335–354.

[13] Liu Cao. "Numerical simulation of the impact of laying powder on selective laser melting single-pass formation". In: *International Journal of Heat and Mass Transfer* 141 (2019), pp. 1036–1048.

[14] X He, PW Fuerschbach, and T DebRoy. "Heat transfer and fluid flow during laser spot welding of 304 stainless steel". In: *Journal of Physics D: Applied Physics* 36.12 (2003), p. 1388.

[15] Wenda Tan, Neil S Bailey, and Yung C Shin. "Numerical modeling of transport phenomena and dendritic growth in laser spot conduction welding of 304 stainless steel". In: *Journal of manufacturing science and engineering* 134.4 (2012).

[16] Ajay Kumar Shukla et al. "Cold model investigations of melting of ice in a gas-stirred vessel". In: *Metallurgical and materials transactions B* 42.1 (2011), pp. 224–235.

[17] YL Hao and Y-X Tao. "Non-thermal equilibrium melting of granular packed bed in horizontal forced convection. Part I: experiment". In: *International journal of heat and mass transfer* 46.26 (2003), pp. 5017–5030.

[18] Jian Yang et al. "Computational study of forced convective heat transfer in structured packed beds with spherical or ellipsoidal particles". In: *Chemical engineering science* 65.2 (2010), pp. 726–738.